# Room temperature strong light-matter coupling in three dimensional terahertz meta-atoms

B. Paulillo, J.-M. Manceau, L. H. Li, A. G. Davies, E. H. Linfield, and R. Colombelli

---

**Articles you may be interested in**

Nanowire photonic crystal waveguides for single-atom trapping and strong light-matter interactions
Appl. Phys. Lett. **104**, 111103 (2014); 10.1063/1.4868975

Strong coupling at room temperature in ultracompact flexible metallic microcavities
Appl. Phys. Lett. **102**, 011118 (2013); 10.1063/1.4773881

Chiral meta-atoms rotated by light
Appl. Phys. Lett. **101**, 031105 (2012); 10.1063/1.4737441

Strong light-matter coupling at terahertz frequencies at room temperature in electronic LC resonators
Appl. Phys. Lett. 97, 191107 (2010); 10.1063/1.3511446

Room temperature enhancement and inhibition of spontaneous emission in semiconductor microcavities
Appl. Phys. Lett. 77, 1345 (2000); 10.1063/1.1290144

---

# Room temperature strong light-matter coupling in three dimensional terahertz meta-atoms

B. Paulillo,[1,a)] J.-M. Manceau,[1,b)] L. H. Li,[2] A. G. Davies,[2] E. H. Linfield,[2] and R. Colombelli[1,c)]

[1]*Institut d'Electronique Fondamentale, Univ. Paris Sud, UMR8622 CNRS, 91405 Orsay, France*
[2]*School of Electronic and Electrical Engineering, University of Leeds, Woodhouse Lane, Leeds LS2 9JT, United Kingdom*

We demonstrate strong light-matter coupling in three dimensional terahertz meta-atoms at room temperature. The intersubband transition of semiconductor quantum wells with a parabolic energy potential is strongly coupled to the confined circuital mode of three-dimensional split-ring metal-semiconductor-metal resonators that have an extreme sub-wavelength volume ($\lambda/10$). The frequency of these lumped-element resonators is controlled by the size and shape of the external antenna, while the interaction volume remains constant. This allows the resonance frequency to be swept across the intersubband transition and the anti-crossing characteristic of the strong light-matter coupling regime to be observed. The Rabi splitting, which is twice the Rabi frequency ($2\Omega_{Rabi}$), amounts to 20% of the bare transition at room temperature, and it increases to 28% at low-temperature. © 2016 AIP Publishing LLC. [http://dx.doi.org/10.1063/1.4943167]

The emerging research field of metamaterial-based devices exploits the electromagnetic response of metamaterials to achieve device functionalities that are otherwise not achievable.[1] Several material systems, including semiconductors and liquid crystals, have been integrated with the metamaterial sub-wavelength building blocks (known as meta-atoms), leading to functionalities such as electro-optic modulation, ultrafast optical modulation, harmonic generation, and bistability.[1] More recently, metasurfaces have been used for cavity electrodynamics with, for example, demonstration of the enhancement of the spontaneous decay rate in a variety of systems (e.g., quantum dots, molecules).[2,3]

The strong-coupling regime between light and matter has also been demonstrated using sub-wavelength resonators and intersubband (ISB) transitions in semiconductor quantum wells (QWs).[4,5] It is known that a reversible energy exchange between light and matter occurs when the interaction coupling constant (the Rabi frequency) is larger than any decay rate of the system. In this situation, new eigenmodes known as ISB polaritons emerge. The combination of metasurfaces and ISB transitions has been exploited for the demonstration of the strong coupling regime in the mid and far-IR ranges of the electromagnetic spectrum,[6–8] as well as for second harmonic generation, and in photodetectors.[9–11] When relying on a planar approach to create polaritonic meta-devices, however, the tuning of the resonator frequency inherently modifies the interaction volume and therefore the number of underlying interacting dipoles. More generally, for an optoelectronic meta-device, one can envisage a well-defined semiconductor spatial region in which an appropriate physical phenomenon takes place (e.g., photoluminescence, detection, and lasing), and which

is combined with an external tuning circuit to adjust the resonant frequency.

In this work, we demonstrate strong light-matter coupling between the fundamental cavity mode of a sub-wavelength, three-dimensional (3D) micro-resonator, and a THz ISB transition. We take advantage of a QW with a parabolic energy potential to enable room temperature (RT) demonstration, which will be important for any future application. Parabolic QWs (PQWs) exhibit absorption independently of the electronic thermal distribution; hence, they can operate at 300 K when the thermal energy $kT$ is larger than the ISB transition energy, as, for instance, demonstrated in Ref. 18. Owing to an innovative micro-fabrication technology exploiting air-bridges, the LC resonance of each micro-resonator can be tuned by *solely* modifying the geometry/ length of the suspended loop antenna (i.e., modifying the inductive section of the device).[12] This allows the characteristic polaritonic anti-crossing behavior to be obtained as a function of the cavity-dipole frequency detuning and enables the volume of the capacitive active region to be kept constant across the entire set of resonant frequencies. Motivated by these results, in the second part of the paper, we discuss the intrinsic energy and field confinement limitations of this resonator architecture in terms of the modal volume. We highlight that a compromise is necessary between the electromagnetic overlap and the minimum modal volume, and we discuss its significance for the development of strongly coupled resonators with small active volumes.

A schematic representation of our split-ring-like 3D meta-atom is shown in Figure 1(a). The capacitive section has a fixed volume and contains a GaAs/Al$_{0.15}$Ga$_{0.85}$As PQW core. The inductive loop antenna's length is lithographically tuned to sweep the frequency of the fundamental LC resonance through the PQW ISB transition frequency. The equivalent circuit is sketched in Figure 1(b): a lumped semiconductor-filled capacitor is connected in parallel with a

a)E-mail: bruno.paulillo@u-psud.fr
b)E-mail: jean-michel.manceau@u-psud.fr
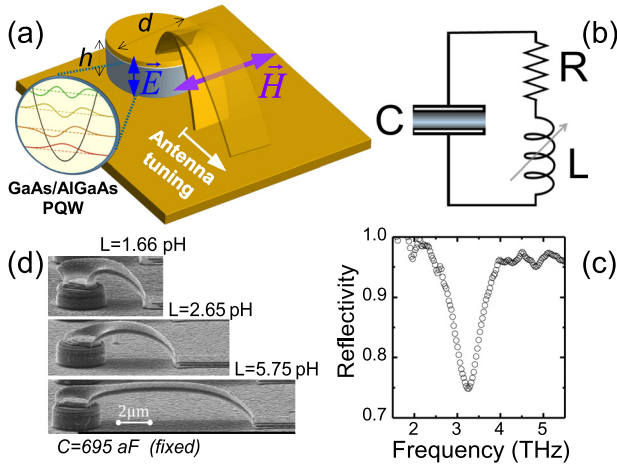c)E-mail: raffaele.colombelli@u-psud.fr

FIG. 1. (a) Schematic diagram of the lithographically tunable LC resonator with an embedded parabolic quantum well. The electric and magnetic dipoles excited by the incoming radiation are shown. The detailed layer structure of the parabolic QW is (in nm): **2.95**/0.15/**2.5**/0.5/**2.04**/0.96/**1.67**/1.33/**1.34**/1.66/**1.04**/1.76/0.2/**0.78**/1.72/0.5/**0.56**/1.94/0.5/**0.37**/2.13/0.5/**0.28**/2.02/0.7/**0.15**/1.85/1/**0.15**/8.1/2/8.1/**0.15**/1/1.85/**0.15**/0.7/2.02/**0.28**/0.5/2.13/**0.37**/0.5/1.94/**0.56**/0.5/1.72/**0.78**/0.2/1.76/**1.04**/1.66/**1.34**/1.33/**1.67**/0.96/**2.04**/0.5/**2.5**/0.15/**14.45**. $Al_{0.15}Ga_{0.85}As$ layers are in bold. Underlined layers are doped to $4 \times 10^{17} \, cm^{-3}$. The structure is repeated 11 times. (b) An equivalent circuit of the LC micro-resonator. (c) A typical reflectivity spectrum of an LC resonator containing undoped GaAs as active core material. The LC resonance, whose FWHM is ≈16%, can be clearly identified. (d) The scanning electron microscope pictures of three LC resonators with different antenna lengths. The top and bottom pictures are the extreme antenna lengths of the overall set, and correspond to the highest and lowest resonator frequencies explored.

tunable inductor, and a series resistor accounts for both radiative and non-radiative losses.[13] A typical reflectivity spectrum of a bare LC resonator containing undoped GaAs as active core material is shown in Figure 1(c). The LC resonance, whose full-width-at-half-maximum (FWHM) is ≈16%, can be clearly identified. The PQW core comprises instead eleven repeated $GaAs/Al_{0.15}Ga_{0.85}As$ PQWs (sample

L1006) grown by molecular beam epitaxy, providing a total sample thickness $h = 1 \, \mu m$. The PQW design is similar to that investigated in Ref. 14, offering an effective parabolic potential. The detailed layer sequence is reported in the caption of Fig. 1. The bare ISB transition of the sample was measured using transmission spectroscopy in a multipass waveguide geometry. A clear absorption peak was identified at 3.6 THz with a FWHM of ≈0.9 THz (see Fig. 2(d)). After standard Au-Au thermo-compressive wafer bonding and substrate removal, the semiconductor heterostructure was patterned into circular mesas of diameter $d = 2.7 \, \mu m$ by ICP-RIE (inductively coupled plasma – reactive ion etching) etching using a Ti/Au/Cr mask. This yields a semiconductor volume of $23 \, \mu m^3$ for each resonator. Suspended Au loop antennas of different lengths were subsequently defined using the technique described in Ref. 12. A series of 16 samples were fabricated with the antenna lengths between $4.65 \, \mu m$ and $11.55 \, \mu m$ (Figure 1(d)). Using the parallel-plate capacitor formula, we estimate the capacitance of each meta-atom to be C = 695 aF (using $\varepsilon_r = 13.4$ for the semiconductor core[15]) while the geometric inductance values range from 1.66 $pH$ to 5.75 $pH$ according to the formula in Ref. 16 (the inductor width and thickness are $w = 2 \, \mu m$ and $t = 0.25 \, \mu m$, respectively). For each different antenna length, $2.5 \times 2.5 \, mm^2$ arrays of meta-atoms (density ≈ 4000 devices/mm²) were fabricated to maximize the overlap with the THz beam. The period of the arrays is sub-wavelength to prevent all diffractive orders except the 0th-order reflection.

Our micro-resonators behave as microscopic LC circuits having separate electric-field (capacitive) and magnetic field (inductive) zones. They are $\lambda/10$ meta-atoms, achieving sub-wavelength confinement in all the three dimensions of space. Frequency tuning is obtained with an external circuital element (the antenna inductance). In this work, we show that it is possible to tune the resonant frequency of the device in
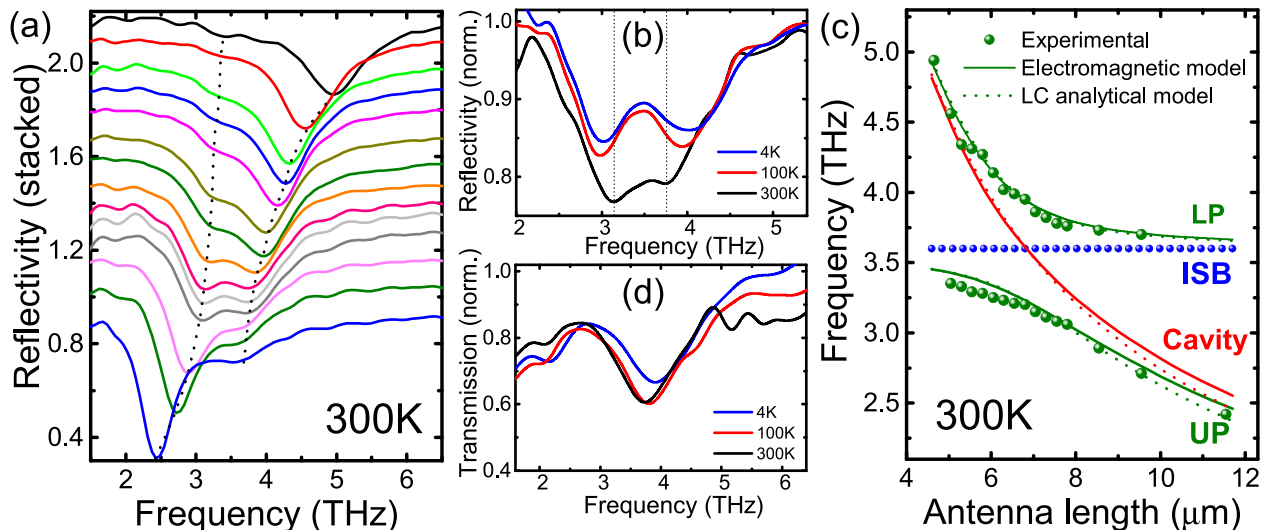


FIG. 2. (a) Experimental reflectivity of the measured devices. The spectra are offset vertically for clarity. The dotted lines are guides to the eye and follow the position of the two polaritonic states. (b) Reflectivity as a function of frequency at different temperatures for the sample with minimum splitting, i.e., at perfect anticrossing. The Rabi splitting at 300 K is 0.7 THz. It increases to 1 THz at 4 K. (c) The experimentally measured reflectivity minima as a function of antenna length (green full circles) corresponding to the frequencies of the polaritonic states. The red lines correspond to the bare cavity resonance obtained with the electromagnetic (full lines) and LC analytical model (dotted line). The full green lines represent the calculated polaritonic frequencies using the electromagnetic model cavity data. The dotted green lines are the calculated polaritonic frequencies using the LC analytical model cavity data. (d) Absorption of the PQW (L1006) measured in a multipass waveguide configuration prior to waferbonding. The measurements have been performed at 4 K, 100 K, and 300 K. The ISB transition FWHM almost does not change with temperature. A slight frequency blue-shift of the transition is observed at 4 K.

and out of the ISB transition acting solely on the inductive element. The antenna is external to the region where the strong light-matter interaction takes place, whose volume—importantly—is kept unvaried. (Additionally, the inductive part of the resonator is fully metallic and free standing and can be in principle modulated/tuned using MEMS techniques.) This is a different objective with respect to the results presented in Refs. 14 and 18. In this case, a planar geometry (i.e., transmission-line resonators) is employed to demonstrate extremely low active volumes, and the frequency tuning is achieved by changing the device's length.

The reflectivity $R(\omega)$ of each sample was measured over a large frequency bandwidth (0.5 to >7 THz) at a fixed angle of 60° using a Fourier transform infrared spectrometer (FTIR) equipped with a Globar thermal source. The incoming radiation was TM-polarized using a wire-grid polarizer (electric field in the plane of incidence), and the reflected signal was measured with a liquid-helium-cooled silicon bolometer. The reflectivity spectrum for each sample was obtained by normalizing the sample spectrum to a reference spectrum obtained from a planar gold surface of the same area. The different experimental configurations for coupling the incident light into this type of resonator have been extensively studied in Ref. 12. Here, we use the highest light coupling configuration as the incoming TM polarization and the sample orientation allow the excitation of both the magnetic and electric dipoles.

The RT experimental results are presented in Figure 2(a) for different inductor lengths. For each sample, two minima (identified by dotted lines) are observed in the reflectivity measurements corresponding to the eigenstates of the system, the ISB polaritons. Owing to the large number of samples, it is possible to resolve the polariton energies as a function of frequency detuning between the cavity mode and the bare ISB transition, and an anti-crossing is observed, which is a clear signature of the strong coupling regime. The smallest frequency splitting (twice the Rabi frequency), measured at the anti-crossing, is equal to 0.70 THz, which represents 20% of the bare ISB transition energy. The sample with the smallest frequency splitting was further investigated as a function of temperature, and the data are shown in Figure 2(b). As the temperature is lowered to 4 K, the reflectivity contrast of the polaritonic branches increases, and the frequency splitting also increases up to 1 THz (28% of the bare transition). This value reflects a device at the onset of the ultra-strong coupling regime that has been already demonstrated in more conventional cavity geometries.[17,18] From the knowledge of the Rabi splitting at a low temperature, which is directly related to the plasma frequency ($\omega_{plasma}$), we can infer a surface electronic density of $4.08 \times 10^{11} \text{ cm}^{-2}$. Doping calibrations have been performed, at low-temperature, on samples grown *before* and *after* sample L1006. They are all consistent, and they provide the value of $4.62 \times 10^{17} \text{ cm}^{-3}$ for the sample real doping. This leads to a surface electronic density of $4.07 \times 10^{11} \text{ cm}^{-2}$, in excellent agreement with the value inferred from the Rabi-splitting at a low temperature.

The observed reduction of the Rabi splitting at RT can be reproduced by a reduced effective doping. The RT polariton energies are plotted in Fig. 2(c) as a function of the measured total antenna length. It is then possible to compare the experimental polaritonic energies with the roots of the following secular equation, which provide the upper and lower polariton frequencies:[19]

$$(\omega^2 - \omega_{cav}^2) \times (\omega^2 - \omega_{12}^2) = \Gamma_{opt}\omega_{plasma}^2\omega_{cav}^2, \qquad (1)$$

where $\omega_{12}$ is the measured ISB transition frequency, $\Gamma_{opt}$ is the electromagnetic overlap, $\omega_{plasma}$ is the electronic plasma frequency in the quantum well, and $\omega_{cav}$ is the cavity frequency (which depends on the antenna size). The bare cavity frequencies are calculated numerically using a commercial finite element modelling software (COMSOL Multiphysics) where the exact sample dimensions are used. Alternatively, a simple LC analytical model can be used, where L and C are estimated based on the sample geometry as described in Refs. 12 and 16. The electromagnetic overlap is extracted from the numerical simulations. It is defined as $\Gamma_{opt} = \int_{AR} |E_z|^2/\int|E|^2$, i.e., the ratio of the squared modulus of the electric field integrated over the active region to the integration over the total volume. We estimate an average value of $\Gamma_{opt} = 0.25$ in our devices. The Rabi splitting being proportional to the square root of the charge density, the measured splitting yields an effective charge density of $2 \times 10^{11} \text{ cm}^{-2}$.

We do not have a definitive explanation for this observation. On one hand, the multipass transmission measurements on sample L1006 prior to waferbonding (Fig. 2(d)) reveal no degradation of the PQW resonance with increasing temperature, thus apparently ruling out the possibility of a reduced available electronic doping at RT. On the other hand, the two device geometries are very different. The multipass waveguide measurements are performed on the mm-sized samples, while the diameter of the LC resonators is 2.7 $\mu$m. The temperature activated surface-depletion-effects could, in principle, reduce the available electronic density at RT.

From the knowledge of the interaction volume and the real charge density, we estimate that each resonator contains $\sim$46 000 electrons. This is about 20 times larger than in mid-IR experiments[6]). The number of interacting dipoles can be reduced by decreasing the active core volume, but the overlap factor $\Gamma_{opt}$ is already far from unity at the current level of field confinement. As demonstrated in Ref. 12, the resonator employed in this work behaves as a lumped-element resonator where the electric and magnetic field spatial regions are well separated. It is therefore useful to determine how $\Gamma_{opt}$ scales with field confinement, since this has a direct impact on the strong coupling regime and, for very low values of $\Gamma$, the system ultimately transitions back to weak coupling.

Figure 3(a) shows the results obtained from numerical simulations. We first estimate the confinement factor for each element of the circuit as a function of the antenna length. The antenna confinement factor is calculated (red full circles) conventionally to be the ratio of the free-space resonance wavelength to the diameter of the hemisphere enclosing the antenna. For comparison, the confinement of the mode in the semiconductor active region (red empty circles) is calculated as the ratio of the effective wavelength in the material, $\lambda_{eff} = \lambda/n_{AR}$, to the mesa diameter. On average, the hybrid resonators provide the typical $\lambda/10$ confinement of split ring resonators, and the confinement—for a fixed capacitor size—is directly dependent on the size of the inductor. In Figure 3(a), the electromagnetic overlap is shown as a
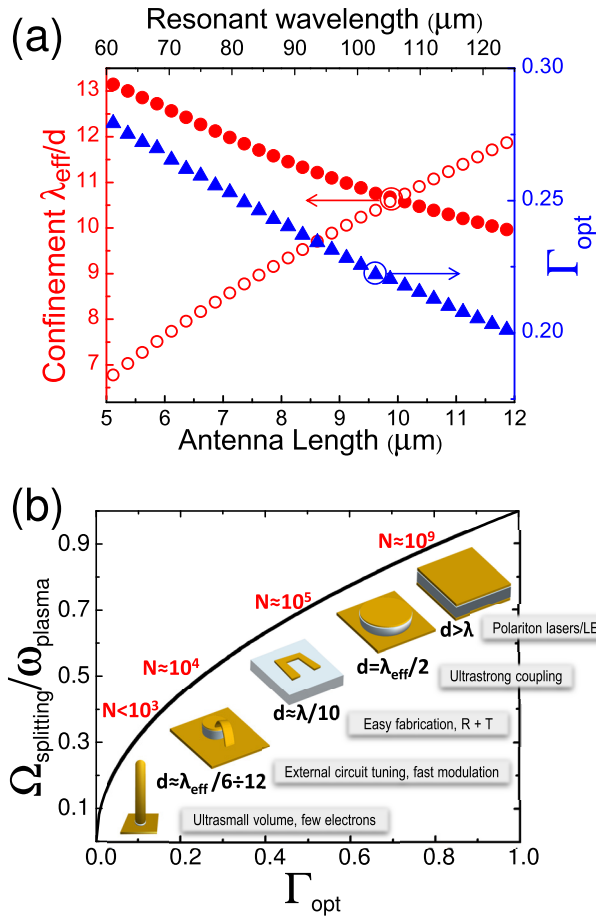
FIG. 3. (a) Calculated confinement and electromagnetic overlap as a function of loop antenna length using FEM software. (b) Ratio of the frequency splitting to the plasma frequency as a function of the electromagnetic overlap for different resonators. For each type of resonator, the number of interacting electrons and the confinement are given qualitatively. We have also added a short description of the application that best suits each resonator architecture.

function of antenna length (blue triangles). The overlap is higher for more compact structures (shorter inductor) and does not exceed $\Gamma_{opt} = 0.3$ for this volume. Note that an improvement in $\Gamma_{opt}$ for a 3D split-ring design could be achieved using high aspect ratio capacitors ($d/h \gg 1$) in order to reduce electric field fringing;[13] for example, employing an ultra-thin semiconductor core (e.g., 100 nm) would yield $\Gamma_{opt} \approx 0.7$. Nevertheless, $\Gamma_{opt}$ will systematically decrease as the active core of the structure progressively decreases to sub-wavelength sizes, in analogy to Figure 3(a). Ultimately, the electromagnetic overlap achievable with wavelength-scale resonators remains unattainable with the metamaterial-based resonators.

We discuss now the perspectives for cavity electrodynamics in sub-wavelength resonators, as a function of their degree of electromagnetic confinement.[21] From the expression for the Rabi splitting ($2\Omega_{Rabi} = \sqrt{\Gamma_{opt}}\omega_{plasma}$), the only resonator-dependent degree of freedom is the electromagnetic overlap $\Gamma_{opt}$. As a consequence, employing sub-wavelength resonators does not bring an improvement in terms of the strength of the light-matter coupling with respect to wavelength-scale structures. Even with an optimum electromagnetic overlap ($\Gamma_{opt} = 1$), the interaction strength is fixed by the plasma frequency of the IST, which is directly proportional to $\sqrt{n_{2D}}$.

However, extremely sub-wavelength resonators provide an opportunity to reduce the number of interacting dipoles, thus allowing the exploration of a few-electron cavity electrodynamics regime, in which processes such as optical bistability and photon-blockade could be achievable.[20] This is shown in Figure 3(b) where different photonic or electronic resonators are classified as a function of their typical $\Gamma_{opt}$. The black curve shows the relative Rabi splitting achievable for a given IST for each design (the $\omega_{plasma}$ value of the PQW employed in this work is used). An estimate of the number $N$ of electrons involved in the light-matter coupling is provided for each resonator as well as its effective confinement. We see that $\Gamma_{opt}$ is close to unity for purely photonic resonators such as mesas,[21] but is reduced to 0.5 for typical planar metamaterials on a quantum-well slab.[7,8] Finally, for 3D structures enclosing an ultra-small semiconductor core, $\Gamma$ is normally reduced down to a few percent, as in the case of vertical out-of-plane monopole antennas.[22] Although the reduction in the interaction active volume permits operation with progressively fewer dipoles, there is a trade-off since the reduction in confinement will be accompanied by a decrease in the frequency splitting, leading ultimately to operation in the weak coupling regime. In essence, each resonator architecture suits specific applications, as reported in the right part of Fig. 3(b). The large size metal-metal mesas suit the development of polariton lasers and light emitting devices (LEDs).[23] Patch-cavities are very interesting for exploring the ultra-strong coupling regime. The planar metamaterials are easier to fabricate and permit to access both reflected *and* transmitted beams. The LC resonators can present peculiar functionalities, thanks to their circuital properties. For instance, since the resonance frequency is fixed by the external circuit, it can be modulated either mechanically (with MEMS) or optically. The latter option is very interesting: if an optical switching element is inserted in the antenna (low-T GaAs, for instance),[24,25] then the resonance frequency could be modulated on ultra-fast timescales offering the opportunity to investigate the dynamic properties of a strong coupling regime. Finally, we believe that the ultimate confinement necessary to explore few-electron systems can be attained using monopolar antennas in an out-of-plane geometry.[22]

In conclusion, we have demonstrated the strong coupling regime between an ISB transition and 3D meta-atoms in the THz frequency range at room temperature. The cavity-matter frequency detuning is obtained via a photolithographic tuning of a suspended loop antenna. Each resonator encloses $\approx 46\,000$ electrons, which interact with the photon field. We have further argued that although the sub-wavelength structures can enable devices where the strong light-matter interaction is achieved with a greatly reduced number of electrons, caution is needed since this is accompanied by a drastic reduction in the optical confinement factor.

[1]N. I. Zheludev and Y. S. Kivshar, Nat. Mater. **11**, 917 (2012).
[2]K. Tanaka, E. Plum, J. Y. Ou, T. Uchino, and N. I. Zheludev, Phys. Rev. Lett. **105**, 227403 (2010).
[3]D. Lu, J. J. Kan, E. E. Fullerton, and Z. W. Liu, Nat. Nanotechnol. **9**, 48 (2014).
[4]M. Helm, in *Intersubband Transitions in Quantum Wells: Physics and Device Applications I*, edited by H. C. Liu and F. Capasso (Elsevier Academic Press, Inc., San Diego, CA, 2000), p. 1.
[5]D. Dini, R. Köhler, A. Tredicucci, G. Biasiol, and L. Sorba, Phys. Rev. Lett. **90**, 116401 (2003).
[6]A. Benz, S. Campione, S. Liu, I. Montaño, J. F. Klem, A. Allerman, J. R. Wendt, M. B. Sinclair, F. Capolino, and I. Brener, Nat. Commun. **4**, 2882 (2013).
[7]G. Scalari, C. Maissen, D. Turčinková, D. Hagenmüller, S. De Liberato, C. Ciuti, C. Reichl, D. Schuh, W. Wegscheider, M. Beck, and J. Faist, Science **335**, 1323 (2012).
[8]D. Dietze, A. Benz, G. Strasser, K. Unterrainer, and J. Darmo, Opt. Express **19**, 13700 (2011).
[9]A. Benz, M. Krall, S. Schwarz, D. Dietze, H. Detz, A. M. Andrews, W. Schrenk, G. Strasser, and K. Unterrainer, Sci. Rep. **4**, 4269 (2014).
[10]O. Wolf, A. A. Allerman, X. Ma, J. R. Wendt, A. Y. Song, E. A. Shaner, and I. Brener, Appl. Phys. Lett. **107**, 151108 (2015).
[11]J. Lee, M. Tymchenko, C. Argyropoulos, P.-Y. Chen, F. Lu, F. Demmerle, G. Boehm, M.-C. Amann, A. Alù, and M. A. Belkin, Nature **511**, 65 (2014).
[12]B. Paulillo, J. M. Manceau, A. Degiron, N. Zerounian, G. Beaudoin, I. Sagnes, and R. Colombelli, Opt. Express **22**, 21302 (2014).

[13]C. A. Balanis, *Antenna Theory: Analysis and Design* (Wiley, 2012).
[14]M. Geiser, C. Walther, G. Scalari, M. Beck, M. Fischer, L. Nevou, and J. Faist, Appl. Phys. Lett. **97**, 191107 (2010).
[15]E. D. Palik, *Handbook of Optical Constants of Solids* (Academic Press, San Diego, CA, 1991).
[16]K. Steinberg, M. Scheffler, and M. Dressel, J. Appl. Phys. **108**, 096102 (2010).
[17]Y. Todorov, A. M. Andrews, R. Colombelli, S. De Liberato, C. Ciuti, P. Klang, G. Strasser, and C. Sirtori, Phys. Rev. Lett. **105**, 196402 (2010).
[18]M. Geiser, F. Castellano, G. Scalari, M. Beck, L. Nevou, and J. Faist, Phys. Rev. Lett. **108**, 106402 (2012).
[19]Y. Todorov and C. Sirtori, Phys. Rev. B **85**, 045304 (2012).
[20]I. Carusotto and C. Ciuti, Rev. Mod. Phys. **85**, 299 (2013).
[21]Y. Todorov, A. M. Andrews, I. Sagnes, R. Colombelli, P. Klang, G. Strasser, and C. Sirtori, Phys. Rev. Lett. **102**, 186402 (2009).
[22]M. Malerba, A. Alabastri, E. Miele, P. Zilio, M. Patrini, D. Bajoni, G. C. Messina, M. Dipalo, A. Toma, R. Proietti Zaccaria, and F. De Angelis, Sci. Rep. **5**, 16436 (2015).
[23]R. Colombelli and J-M. Manceau, Phys. Rev. X **5**, 011031 (2015).
[24]H. T. Chen, W. J. Padilla, J. M. O. Zide, S. R. Bank, A. C. Gossard, A. J. Taylor, and R. D. Averitt, Opt. Lett. **32**, 1620 (2007).
[25]N. H. Shen, M. Massaouti, M. Gokkavas, J.-M. Manceau, E. Ozbay, M. Kafesaki, T. Koschny, S. Tzortzakis, and C. M. Soukoulis, Phys. Rev. Lett. **106**, 037403 (2011).